ACS OMEGA

http://pubs.acs.org/journal/acsodf

Article

Enhanced Effect of an External Electric Field on NH_3BH_3 Dehydrogenation: an AIMD Study for Thermolysis

Yao-Yao Huang, Lin-Xiang Ji, Zheng-Hua He,* and Guang-Fu Ji*

Cite This: *ACS Omega* 2022, 7, 21255−21261

Read Online

ACCESS | Metrics & More | Article Recommendations

ABSTRACT: How to improve the dehydrogenation properties of ammonia borane (AB, NH_3BH_3) is always a challenge for its practical application in hydrogen storage. In this study, we reveal the enhanced effect of an external electric field (E_{ext}) on AB dehydrogenation by means of the ab initio molecular dynamics method. The molecular rotation induced by an electrostatic force can facilitate the formation of the H−N···B−H framework, which would aggregate into poly-BN species and further suppress the generation of the volatile byproducts. Meanwhile, the dihydrogen bond ($N-H^{\delta+}\cdots{}^{\delta-}H-B$) is favorably formed under E_{ext}, and the interaction between relevant H atoms is enhanced, leading to a faster H_2 liberation. Correspondingly, the apparent activation energy for AB dissociation is greatly reduced from 18.42 to around 15 kcal·mol^{-1} with the application of an electric field, while that for H_2 formation decreases from 20.4 to about 16 kcal·mol^{-1}. In the whole process, the cleavage of the B−H bond is more favorable than that of the N−H bond, no matter whether the application of E_{ext}. Our results give a deep insight into a positive effect of an electric field on AB dehydrogenation, which would provide an important inspiration for hydrogen storage in industry applications.

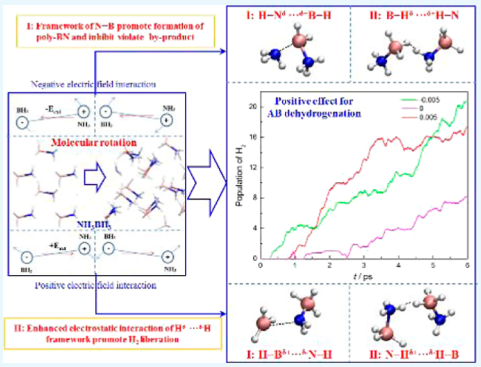

INTRODUCTION

Ammonia borane (NH_3BH_3, AB), as a typical hydrogen-rich material, possesses an extremely high gravimetric and volumetric hydrogen content (19.6 wt % and 0.145 kg·L^{-1}), making it one of the most promising hydrogen storage materials.[1−4] Its unique physical and chemical properties, deriving from the heteropolar dihydrogen bond interaction ($N-H^{\delta+}\cdots{}^{\delta-}H-B$), have attracted extensive attention in relevant fields.[5−8] The classic three-step reaction mechanism (formula 1−3) of AB thermolysis is proposed based on theoretical and experimental studies.[9−11]

$$nNH_3BH_3 \rightarrow (NH_2BH_2)_n + nH_2\ (\sim 108\ ^\circ C,\ 6.5\ wt\ \%) \quad (1)$$

$$(NH_2BH_2)_n \rightarrow (NHBH)_n + nH_2\ (\sim 150\ ^\circ C,\ 6.9\ wt\ \%) \quad (2)$$

$$(NHBH)_n \rightarrow NB + nH_2\ (>500\ ^\circ C,\ 7.3\ wt\ \%) \quad (3)$$

Despite AB seemingly having a moderate reaction temperature, poor dehydrogenation kinetics and many volatile byproducts still hamper its practical application in hydrogen storage.[12,13] To improve the reaction dynamics properties, some special catalysts have been developed and employed to reduce the dehydrogenation energy barrier and depress the impurity formation. For example, Feng et al.[14] investigated the synergistic catalysis of natural halloysite nanotubes and palladium (Pd) nanoparticles on AB decomposition and detected a great improvement for H_2 liberation at a low temperature of 60 °C, with a much lower apparent activation energy of ∼11 kcal·mol^{-1}. Denney et al.[12] reported that the transition metal Ir composite can suppress the formation of byproducts (such as NH_3, B_2H_6, and $B_3N_3H_6$) and catalyze AB thermolysis dehydrogenation. Unfortunately, the remains of catalyst usage are always catastrophic for the recycling of AB regeneration.[15−17] Therefore, it is desirable to develop an efficient and sustainable way for AB dehydrogenation.

Recent research studies reveal that the external electric field (E_{ext}) can significantly adapt the chemical reaction properties without any extra impurity in the system.[18−20] Special orientation of E_{ext} along the "chemical bond/reaction axis" can effectively regulate the global geometric structure and electronic features of the system. The corresponding chemical reactivity and product selectivity can also be improved. Shaik et al.[21] found that NH_3 placed in an $+E_{ext}$ along the z-axis would make it more pyramidal (with a higher dipole moment), whereas reversing the direction of the electric field would cause the molecule to adopt a more planar geometry. Song et al.[22]

Received: April 17, 2022
Accepted: May 31, 2022
Published: June 7, 2022

revealed that the charge transfer between H_2 molecules and the Ca/silicene system is accelerated by applying a positive E_{ext}, which could efficiently facilitate H_2 physical adsorption/desorption. Datta et al.[23] demonstrated that the reactions involving 1,3-dipole aryl-/alkyl-azides and cyclooctyne derivatives can be catalyzed by the application of E_{ext} along the "reaction axis". Similar effects of E_{ext} on the AB system are also detected. Zhang et al.[24] suggested that E_{ext} along the B−N bond axis can lead to variations in the bond length and charge transfer of AB. Wang et al.[25] revealed an "electric dipole" effect generated by the Pt−Ni atoms in the catalytic dehydrogenation process of AB and proposed that the B−H bond is activated by this effect to enhance the dehydrogenation kinetics. Yu et al.[26] reported that the adsorbed B−H bond over the BC_3 sheet was further elongated with E_{ext}, which could greatly promote H_2 production. The promoting effect of the electric field on AB dehydrogenation has been concerned, but the intrinsic interaction mechanism is not sufficiently investigated yet. It is urgent to carry out some necessary studies to promote the practical application of E_{ext} in hydrogen storage.

In this study, we aim to uncover the enhanced effect of E_{ext} on AB dehydrogenation by analyzing the microscopic reaction mechanism and kinetics properties based on ab initio molecular dynamics (AIMD) simulations. We first analyze the structure deformation and electron transfer of AB under E_{ext}. Thereafter, the population evolution of main chemical bonds and key species involved in AB decomposition are discussed to reveal the promoting effects of E_{ext} on AB dehydrogenation. Finally, the reaction kinetics properties are analyzed, and the corresponding kinetics constants are determined.

2. COMPUTATIONAL DETAILS

The thermal decomposition of AB is simulated using the AIMD method implemented in the CP2K code,[27] which is based on a hybrid Gaussian and plane wave method. The exchange−correlation interactions are described using the standard BLYP functional (Becke, Lee−Yang−Parr) with Grimme's dispersion correction.[28,29] A DZVP polarization basis set is employed for DFT calculations. The electron−core interactions are described with a norm conserving Goedecker, Teter, and Hutter[30] pseudopotentials. An energy cutoff of 600 Ry is used for the plane wave expansion for the electron density. The *NVT* ensemble is employed in the AIMD simulation to keep the temperature constant with the Nøse−Hoover thermostat.[31] The van der Waals interaction is considered by DFT-D3.[32]

The initial crystal structure of AB derives from the experimental data, and the low-temperature and low-pressure $Pmn2_1$ phase is picked as a normal theoretical study.[5] It has a typical orthorhombic structure, with the lattice constants of a = 5.395 Å, b = 4.887 Å, and c = 4.986 Å. The cell optimization is first carried out to get the stable structure parameters. The calculated results are a = 5.244 Å, b = 4.737 Å, and c = 4.914 Å, which are well consistent with the experimental data. We start the MD simulation from a 2 × 2 × 3 supercell with 24 AB molecules (Figure 1). The system is relaxed at 200 K for 3 ps to obtain a dynamic equilibration. After that, the temperature is gradually elevated to 2000 K. The external electric fields of 0.0025 and 0.005 au (1 au = 5.14 × 10^{11} V/m) are respectively loaded along the different directions (Figure 1b). The total AIMD simulation time is 6 ps, with a time step of 0.5 fs. The target accuracy for SCF convergence is 10^{-6} au. The MD data are analyzed stepwise using our postprocessing procedure compiled with fortran90.[4] The stable chemical bonds and molecular components are identified by the bond length and lifetime criteria. If the interaction distance of two atoms is smaller than the critical value R_c, and they keep this condition for more than 10 fs, these atoms are considered to be bonded. Here, R_c is determined by the Mulliken bond order of 0.3. Furthermore, any atoms connecting with each other satisfied the above criteria belong to the same molecule.

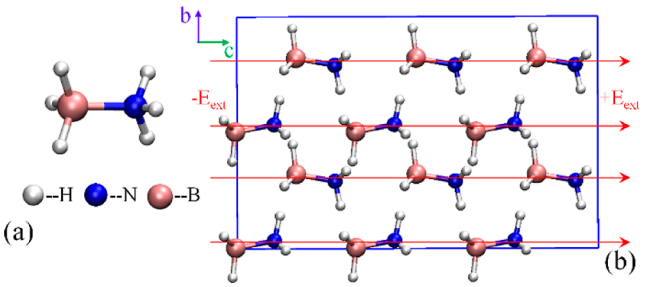

Figure 1. Initial structure of NH_3BH_3 (AB): (a) AB molecule and (b) AB-2 × 2 × 3 supercell.

3. RESULTS AND DISCUSSION

3.1. Structure Deformation and Electron Transfer of AB under an External Electric Field. The chemical bond responses and electron transfer are first investigated when AB is subjected to an external electric field (E_{ext}) at 200 K. Two E_{ext} intensities of 0.0025 and 0.005 au are employed along the *c*-axis direction (Figure 1b). Figure 2a displays the bond length of B−N, B−H, and N−H bonds with different E_{ext}. When the E_{ext} is applied along the c-axis negative direction ($-E_{ext}$, from N atom to B atom), the B−H and N−H bonds shrink with the maximum compression ratios of 0.27 and 0.20%, respectively, while the B−N bond is elongated with a 0.53% increment relative to no E_{ext}. On the contrary, when subjected to the positive direction electric field ($+E_{ext}$, from B atom to N atom), the former two bonds are increased by 0.22 and 0.17%, respectively, while the latter one is decreased by 0.70%. It illustrates that $+E_{ext}$ is beneficial to the activation of B−H and N−H bonds, while $-E_{ext}$ is favorable to that of the B−N bond. Also, the B−N bond is more sensitive to E_{ext}, always with a larger deformation degree. Figure 2b displays the charge transfer between BH_3 and NH_3 groups within AB. It can be seen that $+E_{ext}$ can cause the charge transfer from NH_3 to BH_3, significantly enhancing the N → B dative bond. Inversely, the charge is transferred with the opposite direction under $-E_{ext}$, leading to a weaker B−N bond.

3.2. Population Evolution of Main Chemical Bonds and Key Species. The effect of E_{ext} on AB dehydrogenation is studied at the temperature of 2000 K with an electric field intensity of 0.005 au. Figure 3 shows the population evolutions of B−N, B−H, N−H bonds, and the free H radical. During the first 0.2 ps (subgraph in Figure 3a), the rupture of the B−N bond is more prone under $-E_{ext}$, which indicates the significant activation induced by an electric field. Correspondingly, the breaking of the B−H and N−H bonds is inhibited. These are consistent with the bond length analysis above. After that, a less cleavage for the B−N bond is observed both in conditions of $+E_{ext}$ and $-E_{ext}$ (Figure 3a). Their number even begins to unexpectedly increase from 1.2 ps, while that for the condition

https://doi.org/10.1021/acsomega.2c02401
ACS Omega 2022, 7, 21255−21261

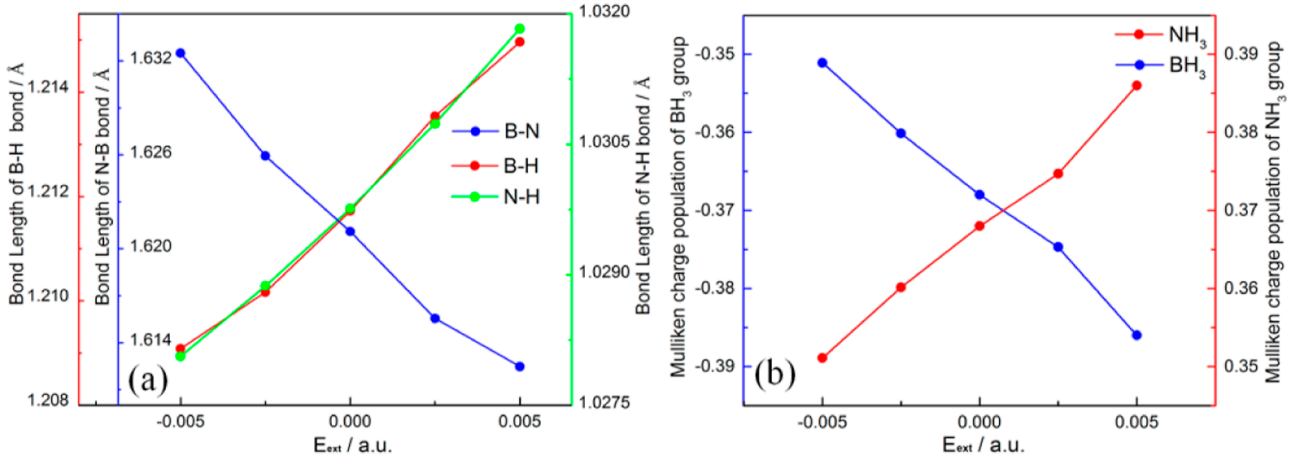

Figure 2. Variations in (a) bond length of B−N, B−H and N−H bonds; (b) Mulliken charge of BH_3 and NH_3 groups vs E_{ext}.

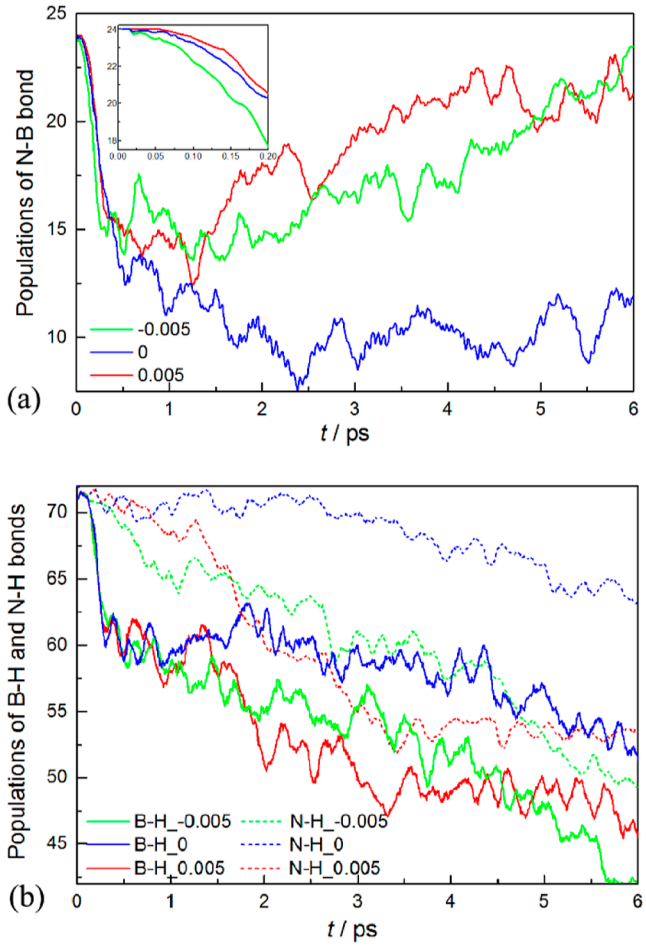

Figure 3. Population evolutions of (a) B−N, (b) B−H, and N−H bonds.

of no electric field application still decreases. It indicates that many new B−N bonds are formed due to the electric field interaction. In contrast, the populations of B−H and N−H bonds decrease continuously, which is more considerable than that without E_{ext}, demonstrating an enhanced effect on dehydrogenation. It is worth noting that no matter whether the application of E_{ext}, the breaking of the B−H bond is always more favorable than that of the N−H bond, especially for the early reaction stage (Figure 3b). It denotes that the B−H bond plays a more important role in AB dehydrogenation, which is consistent with the reaction activity reported in previous work.[33]

The abnormal population evolution of the B−N bond (Figure 3a) is illustrated again by analyzing the reorientation of the AB molecule under a different electric field. As shown in Figure 4a, the backbone of the AB molecule is not rigorously parallel to the direction of E_{ext} at the beginning. The charged BH_3 and NH_3 groups within AB are subjected to different electrostatic forces, which would result in the corresponding rotation of the AB molecule as the arrows represent. Obviously, the moment of force for the system subjected to $-E_{ext}$ can result in more significant molecular rotation than that under $+E_{ext}$ (see the snapshot at 0.15 ps shown in Figure 4b,c). As a result, most AB molecules gradually modulate their orientations to meet the $-E_{ext}$ direction from B to N (see Figure 4, it is just equivalent to that under $+E_{ext}$), and the B−N bond is correspondingly enhanced. Besides, owing to the charged feature of B and N atoms in their individual groups, the similar frameworks of $H-B^{\delta+}\cdots^{\delta-}N-H$ under $+E_{ext}$ and $H-N^{\delta-}\cdots^{\delta+}B-H$ under $-E_{ext}$ are easily formed, which can promote the fragments aggregation to produce poly-BN species. Correspondingly, the volatile byproduct (such as NH_3) is suppressed, and the further dehydrogenation reaction may be enhanced.

Figure 5 displays the population evolutions of the main species involved in AB decomposition. AB molecules subjected to E_{ext} are rapidly depleted within 6 ps, while that for the system without E_{ext} is relatively moderate. As AB is consumed, many NH_3BH_2 fragments and H radicals are produced, while only a little amount of NH_2BH_3 is observed (Figure 5b,c). It also confirms that the initial dehydrogenation mainly starts with a B−H bond cleavage. The newly formed NH_3BH_2 is not stable, which would further dehydrogenation to form NH_2BH_2 (Figure 5d). On the contrary, the H radicals almost maintain a similar dynamic equilibrium after reaching their maximum, but the positive effect of E_{ext} was further confirmed by exploring their different consumption rate in the formation of H_2 in the following section. In addition, although these reactions are all promoted by the application of E_{ext}, the trends of the population change for AB, NH_3BH_2, and NH_2BH_2 display the distinct difference for each E_{ext}. It seems that the system with $-E_{ext}$ has a higher reaction activity at the first ~2 ps, while that with $+E_{ext}$ displays a faster reaction rate after that. It will

https://doi.org/10.1021/acsomega.2c02401
ACS Omega 2022, 7, 21255−21261

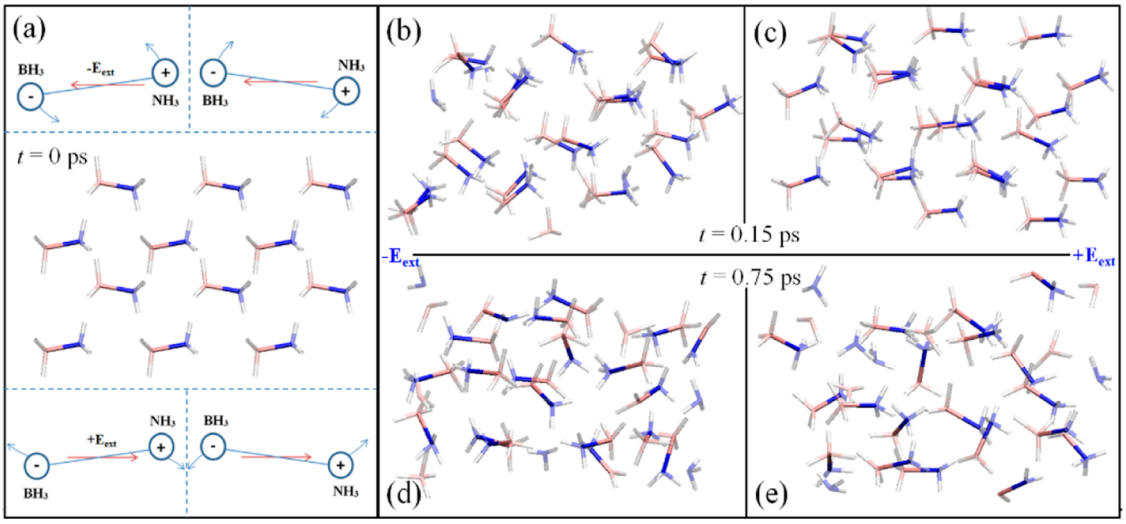

Figure 4. Molecular orientation distribution of AB at (a) 0 ps, (b,c) 0.15 ps, and (d,e) 0.75 ps.

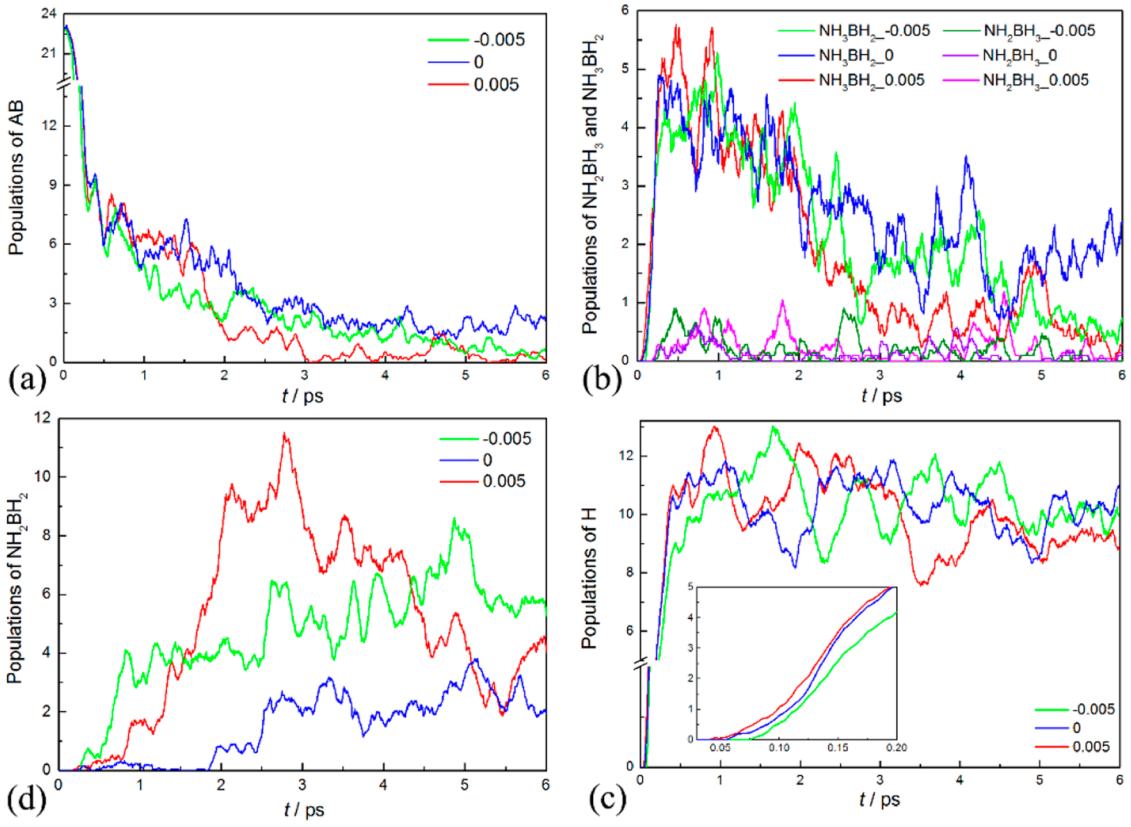

Figure 5. Population evolutions of (a) AB, (b) NH_2BH_3 and NH_3BH_2, (c) H radical, (d) NH_2BH_2.

be further discussed accompanying the microscopic reaction mechanism of H_2 formation.

3.3. Initial H_2 Release Mechanism of AB Thermolysis under an External Electric Field. Figure 6a shows the population evolutions of H_2 molecules within 6 ps. The formation of H_2 under E_{ext} is more favorable than that without E_{ext}, confirming the considerably enhanced effect of E_{ext} on dehydrogenation. A reversal phenomenon of H_2 formation is observed similar to the AB and NH_2BH_2 analyzed above. More H_2 is produced under $-E_{ext}$ at the first 1.5 ps, while an obvious increment of H_2 is observed under $+E_{ext}$ after that. To uncover the intrinsic reason, the dehydrogenation reaction pathways at individual time periods are investigated. The corresponding reaction frequencies are marked in Figure 6a. The heteropolar dihydrogen bond interaction is still the primary dehydrogenation mechanism for AB decomposition, which can be summarized with three typical models: (I) the interaction between $-NBH_3$ and H_3NB-, (II) dominated by BH_4, and (III) dominated by NH_4. Also, the initial formation of H_2 mainly occurs with model-I. As shown in Figure 6b,c, the framework of $N-H^{\delta+}\cdots^{\delta-}H-B$ under $+E_{ext}$ and the framework of $B-H^{\delta-}\cdots^{\delta+}H-N$ under $-E_{ext}$ are ready to be formed, and the interaction between corresponding H atoms is enhanced, which is really beneficial for H_2 liberation. As shown by the

https://doi.org/10.1021/acsomega.2c02401
ACS Omega 2022, 7, 21255−21261

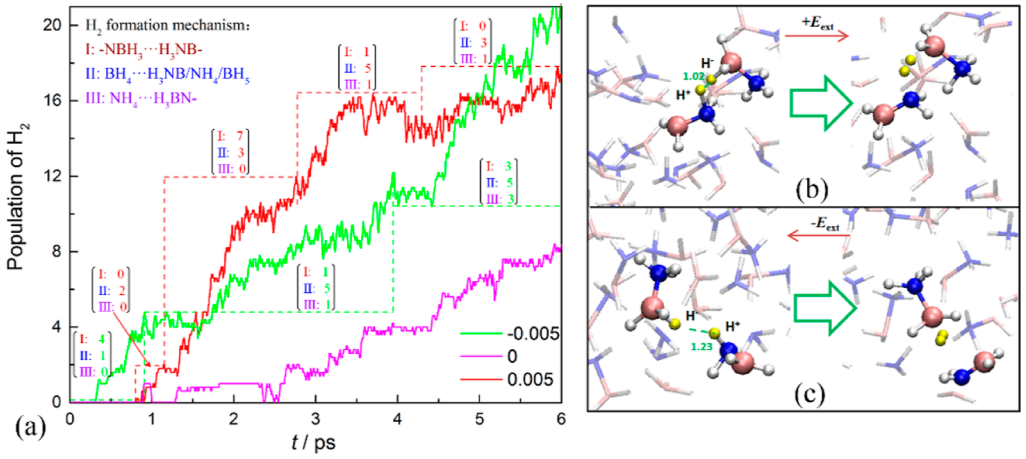

Figure 6. (a) Population evolutions of H_2 vs reaction time (frequencies of dehydrogenation pathways listed in the square brackets); a typical schematic diagram of the H_2 generation mechanism under $+E_{ext}$ (b) and $-E_{ext}$ (c) (the yellow balls represent H atoms involved in the dehydrogenation reaction, and their corresponding distance is labeled with green color).

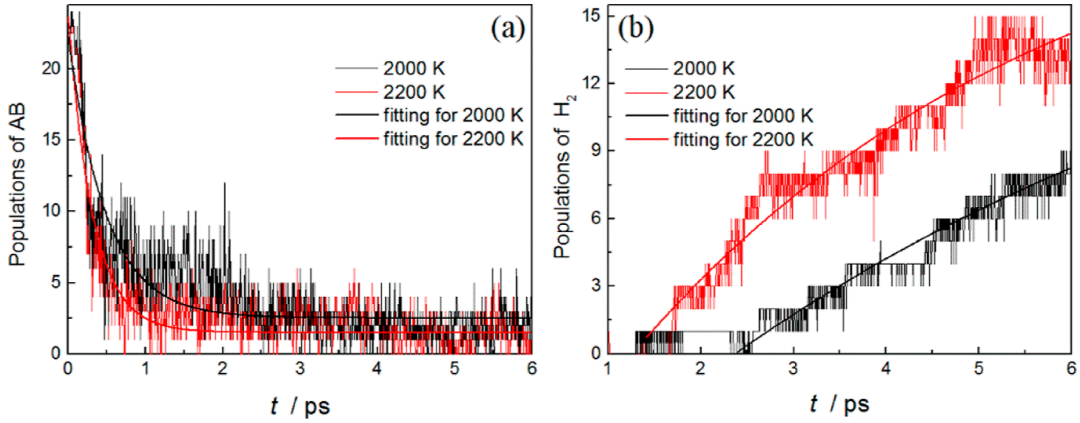

Figure 7. Exponential fitting for populations of ammonia borane (a) and H_2 (b) involved in AB thermolysis.

analysis in Section 3.2 (Figure 4), the molecule rotation caused by the moment of force under $-E_{ext}$ is more significant at an early stage. The framework of $B-H^{\delta-}\cdots^{\delta+}H-N$ is preferential to form, which would directly induce a faster and earlier formation of H_2. However, after 0.75 ps (Figure 4d), many AB molecules complete their reorientation, and the initial rotation advantage is not considerable. Owing to the coupling interaction of the temperature and electric field under $+E_{ext}$, the molecular orientation deviates from the horizontal axis (Figure 4e). Also, the following molecule reorientation easily promotes the formation of the $N-H^{\delta+}\cdots^{\delta-}H-B$ framework, resulting in a fast formation of H_2 (Figure 6a). Despite that, the equivalent effects of different electric fields on the initial dehydrogenation reaction through the dihydrogen bond framework are confirmed, which mainly derive from the molecular reorientation as shown in Figure 4.

In addition, the initial dihydrogen bond frameworks are mainly produced between NH_3BH_3, NH_2BH_3, and NH_3BH_2 molecules, leading to the accompanying formation of H_2 and NH_2BH_2. That is why the population evolution trends of them almost keep consistent with each other (Figures 5c and 6a). As the reaction proceeds, many active radicals of NH_4 and BH_4 are formed. The special dihydrogen bond interactions dominated by them become the main reaction pathways for H_2 liberation (Figure 6a). Also, the BH_4 groups obviously possess a higher reaction activity than that of NH_4 in this dehydrogenation process, also identifying the more important role of the B−H bond. Besides, we also observe another reaction pathway with H radical adsorbed on B ends to form the pentacoordinate boron-containing species, such as BH_5. The extra H combination obviously activates the adjacent B−H bond. Accordingly, two B−H bonds are elongated and further break to release the H_2 molecule. Although a similar reaction pathway is also observed in the previous theoretical study under shock loading,[4] the H radical mainly derives from N ends through a heteropolar dihydrogen bond interaction in this work. It further confirms the importance of the heteropolar dihydrogen bond under E_{ext}.

3.4. Reaction Dynamics Properties for AB Thermal Decomposition. To reveal the reaction dynamics properties, we add the other three simulations for AB thermolysis under 2200 K with a relevant E_{ext}. The results show that the population evolution for main species always complies with a typical exponential form. The numbers of AB molecules and B−N, B−H, and N−H bonds can be fitted with formula 4 in their dissociation reaction stage, while that for H_2 formation can be fitted with formula 5, respectively.

$$C_{(t)} = C_0 \cdot \exp(-b \cdot t) + c \tag{4}$$

$$C_{(t)} = C_\infty \cdot (1 - \exp(-b \cdot (t - c))) \tag{5}$$

https://doi.org/10.1021/acsomega.2c02401
ACS Omega 2022, 7, 21255−21261

Here, parameter b is just the reaction rate constant when subjected to the first-order model[34] and can be directly determined by an exponential fitting. Figure 7a,b displays an example for the curve fitting of the populations of AB and H_2 without an electric field. It shows a good agreement between the fitting curve and the original data. To further obtain the kinetics characteristics, we employ the classical Arrhenius equation ($k = A{\cdot}\exp(-E_a/RT)$) to fit the reaction rate constant. The individual reaction activation energies are obtained by linear fitting of its natural logarithm form ($\ln(k) = \ln(A) - E_a/RT$) and are listed in Table 1. The apparent activation energies with no application of electric field calculated in our study are from 18.42 to 30.17 kcal·mol^{-1}, which are comparable with the previous experimental results (21.98 to 35.24 kcal·mol^{-1}) proposed by Gangal and Sharma[35] However, a significant reduction for all the energy barriers are detected when subjected to E_{ext}, which confirms a definite enhancement of the dehydrogenation kinetics. No significant distinct is observed with the different orientations of E_{ext}, which may be ascribed to the similar reaction form deriving from the molecular rotation and reorientation, as discussed in Section 3.2. Among them, the apparent activation energy for AB decomposition is reduced from 18.42 to around 15 kcal·mol^{-1} with E_{ext}, while that for H_2 formation decreases from 20.40 to about 16 kcal·mol^{-1}. The breaking of the B−H bond has the approximate values with the former two, indicating a much closer relationship with H_2 liberation. However, the cleavage of the N−H bond requires overcoming much higher energy barriers of 30.17, 21.09, and 19.62 kcal·mol^{-1} for different conditions. It indicates that N−H breaking may be the rate control step for H_2 formation.

Table 1. Apparent Activation Energies for Different Reactions in AB Thermolysis

E_a/(kcal·mol^{-1})		AB	B−N	B−H	N−H	H_2
electric field (a.u.)	0	18.42	21.32	18.98	30.17	20.40
	0.005	15.62	18.51	15.46	21.09	16.36
	−0.005	14.86	18.06	14.38	19.62	16.16

4. CONCLUSIONS

In summary, we systematically investigated the effect of an external electric field (E_{ext}) on AB dehydrogenation using the AIMD method. The rupture of the N−B bond is inhibited, and more H radicals are formed when subjected to $+E_{ext}$ at the early stage, while it does the opposite under $-E_{ext}$. As the coupling interaction of the temperature and electric field, the significant molecular rotation promotes the formation of the H−B$^{\delta+}$···$^{\delta-}$N−H framework under $+E_{ext}$ and the H−N$^{\delta-}$···$^{\delta+}$B−H framework under $-E_{ext}$, which are beneficial for the fragment aggregation and suppress the formation of the volatile byproducts. More importantly, the positive effect of E_{ext} on AB dehydrogenation is revealed by analyzing the microscopic reaction mechanism. The H_2 molecule is favorably produced by the formation of the framework of N−H$^{\delta+}$···$^{\delta-}$H−B under $+E_{ext}$ or B−H$^{\delta-}$···$^{\delta+}$H−N under $-E_{ext}$. Also, the BH_4 and NH_4 fragments would dominate the H_2 liberation after the AB molecule rupture. During the whole process, the breaking of the B−H bond is always more favorable than that of the N−H bond, no matter whether the application of E_{ext}. Besides, the obvious enhanced effect of the electric field on dehydrogenation kinetics is detected, with the apparent activation energy for H_2 formation reduced from 20.40 to around 16 kcal·mol^{-1}. Our work provides a deep understanding of the enhancement of AB dehydrogenation properties under an electric field, which would promote its practical application in hydrogen storage.

AUTHOR INFORMATION

Corresponding Authors

Zheng-Hua He − *National Key Laboratory of Shock Wave and Detonation Physics, Institute of Fluid Physics, China Academy of Engineering Physics, Mianyang 621900 Sichuan, China*; orcid.org/0000-0002-5764-5972; Phone: 0086-0816-2495259; Email: herary-hezhh@caep.cn

Guang-Fu Ji − *National Key Laboratory of Shock Wave and Detonation Physics, Institute of Fluid Physics, China Academy of Engineering Physics, Mianyang 621900 Sichuan, China*; Phone: 0086-0816-2485108; Email: cyfjkf@126.com

Authors

Yao-Yao Huang − *National Key Laboratory of Shock Wave and Detonation Physics, Institute of Fluid Physics, China Academy of Engineering Physics, Mianyang 621900 Sichuan, China*

Lin-Xiang Ji − *Department of Physics and Engineering Physics, University of Saskatchewan, Saskatoon, Saskatchewan S7N5E2, Canada*

Complete contact information is available at: https://pubs.acs.org/10.1021/acsomega.2c02401

Notes

The authors declare no competing financial interest.

ACKNOWLEDGMENTS

This research was funded by the National Natural Science Foundation of China (no. 11902307).

REFERENCES

(1) Hamilton, C. W.; Baker, R. T.; Staubitz, A.; Manners, I. B−N Compounds for Chemical Hydrogen Storage. *Chem. Soc. Rev.* **2009**, *38*, 279−293.

(2) Wang, P.; Kang, X.-d. Hydrogen-Rich Boron-Containing Materials for Hydrogen Storage. *Dalton Trans.* **2008**, 5400−5413.

(3) Demirci, U. B. Mechanistic Insights into the Thermal Decomposition of Ammonia Borane, a Material Studied for Chemical Hydrogen Storage. *Inorg. Chem. Front.* **2021**, *8*, 1900−1930.

(4) Huang, Y.-Y.; Ji, L.-X.; Shi, L.-T.; Ren, H.-C.; He, Z.-H.; Ji, G.-F. Dehydrogenation and Rehydrogenation of Ammonia Borane under Shock Loading: Ab Initio Molecular Dynamics Simulations. *J. Phys. Chem. C* **2020**, *124*, 27300−27308.

(5) Klooster, W. T.; Koetzle, T. F.; Siegbahn, P. E. M.; Richardson, T. B.; Crabtree, R. H. Study of the N−H···H−B Dihydrogen Bond Including the Crystal Structure of BH_3NH_3 by Neutron Diffraction. *J. Am. Chem. Soc.* **1999**, *121*, 6337−6343.

(6) Morrison, C. A.; Siddick, M. M. Dihydrogen Bonds in Solid BH_3NH_3. *Angew. Chem., Int. Ed.* **2004**, *43*, 4780−4782.

(7) Custelcean, R.; Dreger, Z. A. Dihydrogen Bonding under High Pressure: A Raman Study of BH_3NH_3 Molecular Crystal. *J. Phys. Chem. B* **2003**, *107*, 9231−9235.

(8) Demirci, U. B. Ammonia Borane, a Material with Exceptional Properties for Chemical Hydrogen Storage. *Int. J. Hydrogen Energy* **2017**, *42*, 9978−10013.

https://doi.org/10.1021/acsomega.2c02401
ACS Omega 2022, 7, 21255−21261

(9) Liang, Y.; Tse, J. S. First-Principles Study on the Mechanisms for H_2 Formation in Ammonia Borane at Ambient and High Pressure. *J. Phys. Chem. C* **2012**, *116*, 2146−2152.
(10) Rizzi, V.; Polino, D.; Sicilia, E.; Russo, N.; Parrinello, M. The Onset of Dehydrogenation in Solid Ammonia Borane: An Ab Initio Metadynamics Study. *Angew. Chem., Int. Ed.* **2019**, *58*, 3976−3980.
(11) Lin, Y.; Mao, W. L. High-Pressure Storage of Hydrogen Fuel: Ammonia Borane and Its Related Compounds. *Chin. Sci. Bull.* **2014**, *59*, 5235−5240.
(12) Denney, M. C.; Pons, V.; Hebden, T. J.; Heinekey, D. M.; Goldberg, K. I. Efficient Catalysis of Ammonia Borane Dehydrogenation. *J. Am. Chem. Soc.* **2006**, *128*, 12048−12049.
(13) Rossin, A.; Peruzzini, M. Ammonia−Borane and Amine−Borane Dehydrogenation Mediated by Complex Metal Hydrides. *Chem. Rev.* **2016**, *116*, 8848−8872.
(14) Feng, Y.; Zhou, X.; Yang, J.-h.; Gao, X.; Yin, L.; Zhao, Y.; Zhang, B. Encapsulation of Ammonia Borane in Pd/Halloysite Nanotubes for Efficient Thermal Dehydrogenation. *ACS Sustainable Chem. Eng.* **2020**, *8*, 2122−2129.
(15) Yao, Q.; Yang, K.; Hong, X.; Chen, X.; Lu, Z.-H. Base-Promoted Hydrolytic Dehydrogenation of Ammonia Borane Catalyzed by Noble-Metal-Free Nanoparticles. *Catal. Sci. Technol.* **2018**, *8*, 870−877.
(16) Hou, C.-C.; Li, Q.; Wang, C.-J.; Peng, C.-Y.; Chen, Q.-Q.; Ye, H.-F.; Fu, W.-F.; Che, C.-M.; López, N.; Chen, Y. Ternary Ni−Co−P Nanoparticles as Noble-Metal-Free Catalysts to Boost the Hydrolytic Dehydrogenation of Ammonia-Borane. *Energy Environ. Sci.* **2017**, *10*, 1770−1776.
(17) Lu, Z.; Schweighauser, L.; Hausmann, H.; Wegner, H. A. Metal-Free Ammonia−Borane Dehydrogenation Catalyzed by a Bis(Borane) Lewis Acid. *Angew. Chem., Int. Ed.* **2015**, *54*, 15556−15559.
(18) Gondo, A.; Manabe, R.; Sakai, R.; Murakami, K.; Yabe, T.; Ogo, S.; Ikeda, M.; Tsuneki, H.; Sekine, Y. Ammonia Synthesis over Co Catalyst in an Electric Field. *Catal. Lett.* **2018**, *148*, 1929−1938.
(19) Ogino, K.; Sasaki, Y.; Kurosawa, Y.; Ogo, S.; Yabe, T.; Kondo, W.; Ono, T.; Kojima, K.; Sekine, Y. Hydrogen Production by Water Decomposition through Redox Reaction of Ce-Based Metal Oxide Systems in Electric Field. *Chem. Lett.* **2018**, *47*, 643−646.
(20) Sekine, Y.; Yamagishi, K.; Nogami, Y.; Manabe, R.; Oshima, K.; Ogo, S. Low Temperature Catalytic Water Gas Shift in an Electric Field. *Catal. Lett.* **2016**, *146*, 1423−1428.
(21) Shaik, S.; Ramanan, R.; Danovich, D.; Mandal, D. Structure and Reactivity/Selectivity Control by Oriented-External Electric Fields. *Chem. Soc. Rev.* **2018**, *47*, 5125−5145.
(22) Song, E. H.; Yoo, S. H.; Kim, J. J.; Lai, S. W.; Jiang, Q.; Cho, S. O. External Electric Field Induced Hydrogen Storage/Release on Calcium-Decorated Single-Layer and Bilayer Silicene. *Phys. Chem. Chem. Phys.* **2014**, *16*, 23985−23992.
(23) Bhattacharyya, K.; Karmakar, S.; Datta, A. External Electric Field Control: Driving the Reactivity of Metal-Free Azide−Alkyne Click Reactions. *Phys. Chem. Chem. Phys.* **2017**, *19*, 22482−22486.
(24) Zhang, X.; Sun, S.-L.; Xu, H.-L.; Su, Z.-M. Ammonia Borane in an External Electric Field: Structure, Charge Transfer, and Chemical Bonding. *RSC Adv.* **2015**, *5*, 65991−65997.
(25) Wang, B.; Xiong, L.; Hao, H.; Cai, H.; Gao, P.; Liu, F.; Yu, X.; Wu, C.; Yang, S. The "Electric-Dipole" Effect of Pt-Ni for Enhanced Catalytic Dehydrogenation of Ammonia Borane. *J. Alloys Compd.* **2020**, *844*, 156253.
(26) Yu, J.; He, C.; Huo, J.; Zhao, C.; Yu, L. Adsorption and Electric Field Assisted Activation of Ammonia -Borane over BC_3 Sheet: A Computational Study. *Int. J. Hydrogen Energy* **2022**, *47*, 7738−7750.
(27) Vandevondele, J.; Krack, M.; Mohamed, F.; Parrinello, M.; Chassaing, T.; Hutter, J. Quickstep: Fast and Accurate Density Functional Calculations Using a Mixed Gaussian and Plane Waves Approach. *Comput. Phys. Commun.* **2005**, *167*, 103−128.
(28) Lee, C.; Yang, W.; Parr, R. G. Development of the Colle-Salvetti Correlation-Energy Formula into a Functional of the Electron Density. *Phys. Rev. B: Condens. Matter Mater. Phys.* **1988**, *37*, 785−789.
(29) Becke, A. D. Density-Functional Exchange-Energy Approximation with Correct Asymptotic Behavior. *Phys. Rev. A* **1988**, *38*, 3098−3100.
(30) Goedecker, S.; Teter, M.; Hutter, J. Separable Dual-Space Gaussian Pseudopotentials. *Phys. Rev. B: Condens. Matter Mater. Phys.* **1996**, *54*, 1703−1710.
(31) Nosé, S. A Molecular-Dynamics Method for Simulations in the Canonical Ensemble. *Mol. Phys.* **1984**, *52*, 255−268.
(32) Grimme, S. Supramolecular Binding Thermodynamics by Dispersion-Corrected Density Functional Theory. *Chem.—Eur. J.* **2012**, *18*, 9955−9964.
(33) Petit, J.-F.; Demirci, U. B. Mechanistic Insights into Dehydrogenation of Partially Deuterated Ammonia Borane NH_3BD_3 Being Heating to 200 °C. *Inorg. Chem.* **2019**, *58*, 489−494.
(34) He, Z.-H.; Yu, Y.; Huang, Y.-Y.; Chen, J.; Wu, Q. Reaction Kinetic Properties of 1,3,5-Triamino-2,4,6-Trinitrobenzene: A DFTB Study of Thermal Decomposition. *New J. Chem.* **2019**, *43*, 18027−18033.
(35) Gangal, A. C.; Sharma, P. Kinetic Analysis and Modeling of Thermal Decomposition of Ammonia Borane. *Int. J. Chem. Kinet.* **2013**, *45*, 452−461.

https://doi.org/10.1021/acsomega.2c02401
ACS Omega 2022, 7, 21255−21261